PHYSICAL REVIEW B **75**, 041309(R) (2007)

Mixing of two-electron spin states in a semiconductor quantum dot

Ş. C. Bădescu and T. L. Reinecke
Naval Research Laboratory, Washington DC 20375, USA

(Received 22 September 2006; revised manuscript received 13 December 2006; published 31 January 2007)

We show that the low-lying spin states of two electrons in a semiconductor quantum dot can be strongly mixed by electron-electron asymmetric exchange. This mixing is generated by the coupling of the electron spin to its orbital motion and to the relative orbital motion of the two electrons. The asymmetric exchange can be as large as 50% of the isotropic exchange, even for cylindrical dots. The resulting mixing can contribute to understanding spin dynamics in dots, such as recent observations of light polarization reversal.

DOI: 10.1103/PhysRevB.75.041309 PACS number(s): 73.21.La, 71.35.Pq, 71.70.Ej, 71.70.Gm

An electron spin in a semiconductor quantum dot (QD) is an attractive qubit for quantum computing:[1] the spin in the ground orbital state can have a long coherence time;[2] a single qubit can be initialized or read optically by transient electron-hole pair excitation giving a negative trion X^-;[3,4] and the manipulation of the spin exchange between spins can be the basis for two-qubit gates.[1] The correlations between spins control coherence in gates. The dominant interaction between two electrons (*e-e*) is the symmetric exchange $J\hat{\boldsymbol{s}}_1\cdot\hat{\boldsymbol{s}}_2$, which conserves the total spin $\hat{\boldsymbol{S}}$. Additional spin-asymmetric *e-e* interactions (asymmetric exchange) do not conserve $\hat{\boldsymbol{S}}$ and can cause decoherence.

Examples of recent experiments on spin dynamics are those involving optical polarization reversal.[3,4] They involve spin flipping due to electron-hole (*e-h*) exchange in QDs with lateral asymmetry. It has been noted that those experiments require strong spin mixing, inconsistent with *e-h* exchange alone.[4]

Spin-orbit (SO) interactions play a key role in the mixing of spin states. They arise from effective magnetic fields of the orbital motion of electrons.[5] Electrons in QD ground states with dominant *s* components have small orbital angular momentum and small SO coupling. A number of experiments involve electrons in excited states. Linear combinations of nearly degenerate excited states in a plane (e.g., p_x- and p_y-like) can give rise to two-dimensional (2D) orbital motion with an effective magnetic field perpendicular to the plane, and thus to large SO coupling. This is analogous to the $\hat{\boldsymbol{L}}\cdot\hat{\boldsymbol{S}}$ coupling in atoms. Thus, symmetric QDs (e.g., cylindrical) can have significant SO effects.

There are three sources of SO coupling that lead to mixing of spin states. The largest two contributions arise from the $\boldsymbol{k}\cdot\hat{\boldsymbol{p}}$ mixing of the conduction and valence bands and can be described in the effective mass approximation.[6] We derive them by treating the potentials from the structure and the *e-e* Coulomb repulsion on the same footing with $\boldsymbol{k}\cdot\hat{\boldsymbol{p}}$ terms using the Kane model.[7] We have in mind QDs with a strong confinement in a single state $\xi(z)$ in the vertical direction $\boldsymbol{e}_z$ and weaker confinement in the transverse directions, which gives the single-particle electron states $\phi_i(\boldsymbol{r})=\xi(z)\varphi_i(\boldsymbol{\rho})$.

A single-electron contribution to the SO coupling, $\hat{\boldsymbol{h}}^V$, arises from the 2D *structure potential* $V(\boldsymbol{r})$:[8]

$$\hat{\boldsymbol{h}}^V\cdot\hat{\boldsymbol{s}}=\gamma_s^V[\partial_z V(\hat{\boldsymbol{p}}^\perp\times\hat{\boldsymbol{s}}^\perp)+(\partial_{\boldsymbol{\rho}}V\times\hat{\boldsymbol{p}}^\perp)\hat{s}^z]\boldsymbol{e}_z. \tag{1}$$

$\hat{p}^z$ is not present due to the strong vertical confinement [for a single state $\xi(z)$, $\langle\xi|p^z|\xi\rangle=0$]. The first term is the usual Rashba coupling $\gamma^V(\boldsymbol{e}_z\times\hat{\boldsymbol{p}}^\perp)$ from the asymmetry in the growth direction,[9] where $\gamma^V=\gamma_s^V\langle\xi|\partial_z V|\xi\rangle$.[10] The second term is important between (almost) degenerate excited states, e.g., p_x- and p_y-like, where it gives the dominant SO coupling independent of structure or bulk inversion asymmetry; it is negligible in the ground state, whose main component is inversion symmetric (*s*-like).

The second contribution, $\hat{\boldsymbol{h}}^C$, is from the interaction of each spin with the other electron's orbital motion. We obtain it using a two-particle $\boldsymbol{k}\cdot\hat{\boldsymbol{p}}$ approach for electrons interacting through the *Coulomb potential*[11] $U_C(\boldsymbol{r}_r)=e^2/\kappa\boldsymbol{r}_r$ (κ is the dielectric constant; $\boldsymbol{r}_r=\boldsymbol{r}_1-\boldsymbol{r}_2$):

$$\hat{\boldsymbol{h}}_k^C\cdot\hat{\boldsymbol{s}}_k=(-1)^k\gamma_s(\boldsymbol{\nabla}_{\boldsymbol{r}_r}U_C\times\hat{\boldsymbol{p}}_k)\cdot\hat{\boldsymbol{s}}_k, \tag{2}$$

where $k=1,2$. $\hat{\boldsymbol{h}}^V$ is analogous to the Pauli SO interaction, while $\hat{\boldsymbol{h}}^C$ is analogous to the Breit-Pauli spin–relative-orbit coupling.[5] These couplings in vacuum or in atoms are relativistically small due to the large energy gap $2m_0c^2$ between electron and positron bands, whereas the present gap E_g is smaller giving larger SO couplings.

A smaller contribution, $\hat{\boldsymbol{h}}^{\mathrm{B}}$, comes from the *Dresselhaus coupling* due to the lack of bulk inversion symmetry.[12] It arises from the mixing of the conduction band with the remote upper bands. In QDs with strong vertical confinement [$\langle p^{z2}\rangle\gg\langle p^{\perp 2}\rangle$], it reduces to $\boldsymbol{h}^{B,\perp}\simeq\gamma^B(\hat{p}_x,-\hat{p}_y)$, where $\gamma^B=\gamma_b^B\langle\xi|p_z^2|\xi\rangle$.[12]

We use a model[13] of QDs like those from self-assembled growth along the crystal axis [001]. The lateral potential $\mathcal{V}(\boldsymbol{\rho})$ contains $\mathcal{V}_s$ symmetric for the inversion $\boldsymbol{\rho}\to-\boldsymbol{\rho}$, and it may also contain an inversion-asymmetric part $\mathcal{V}_a$. The lateral parameters $D_{x,y}$ of the potential provide a measure for the QD size. A nonzero asymmetry $\mathcal{V}_a=\mathcal{V}_{ax}+\mathcal{V}_{ay}$ ($\mathcal{V}_{ax}$ odd in x, and $\mathcal{V}_{ay}$ odd in y) implies a nonzero average lateral electric field $\bar{\mathcal{E}}_{x,y}$. The inversion asymmetry is parametrized in $\mathcal{V}_{ax}$ by E_x, and in $\mathcal{V}_{ay}$ by E_y. We can write $\bar{\mathcal{E}}_{x,y}\propto E_{x,y}/D_{x,y}$.[13]

First, we consider the orbital eigenstates of the two-particle Hamiltonian H_0 containing the Coulomb interaction U_C but not the SO couplings. H_0 has an inversion-symmetric part $(\hat{\boldsymbol{p}}_1^{\perp 2}+\hat{\boldsymbol{p}}_2^{\perp 2})/2m+\mathcal{V}_s(\boldsymbol{\rho}_1)+\mathcal{V}_s(\boldsymbol{\rho}_2)+U_C(\boldsymbol{r}_r)+\gamma_c\delta(\boldsymbol{r}_r)$, and an inversion-asymmetric part $\mathcal{V}_a(\boldsymbol{\rho}_1)+\mathcal{V}_a(\boldsymbol{\rho}_2)$. From their permutation symmetry, the eigenstates are separated into triplets $\{T_i\}$ (asymmetric) and singlets $\{S_j\}$ (symmetric). We build a basis for each group from products of single-particle wave functions. We use a large set of harmonic oscillator wave functions obtained from the average curvatures of the

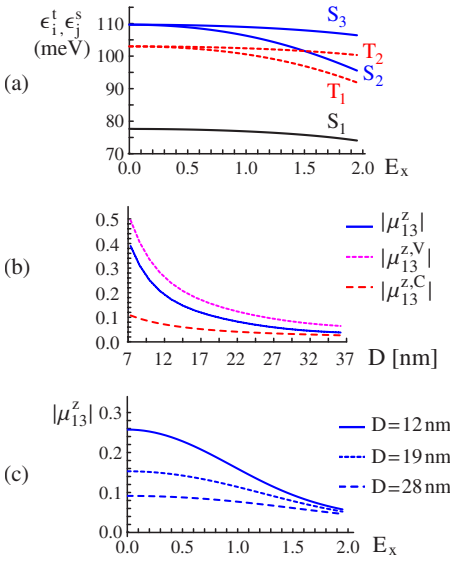

FIG. 1. (Color online) QDs with diameters $D_x=D_y=D$. (a) Two-electron energy levels in QDs with $D=19$ nm with one plane of symmetry along $\boldsymbol{e}_x$ ($E_y=0$) vs the lateral asymmetry parameter E_x (the average field is $\bar{\mathcal{E}}_x=10.1E_x$ meV/nm). (b) The asymmetric exchange $|\mu_{13}^z|=\hbar^{-1}|\beta_{13}^z/J_{13}|$ and its components $|\mu_{13}^{z,V}|$ (from the SO coupling [Eq. (1)]), $|\mu_{13}^{z,C}|$ (from the spin–relative-orbit coupling [Eq. (2)]) vs the QD size D. (c) $|\mu_{13}^z|$ vs E_x ($E_y=0$) for several QDs.

potential and grouped in four subspaces {s}, {x}, {y}, and {d}, by their orbital symmetry: s symmetry (even in x and y), x (odd in x), y (odd in y), d (odd in x and y). The triplet basis $\{\tau_m\}$ contains asymmetric combinations such as $\tau_{sx}=(sx-xs)/\sqrt{2}$, and has four independent subspaces, of symmetry s, x, y, and d: $\{\tau_{ss'},\tau_{xx'},\tau_{yy'},\tau_{dd'}\}$, $\{\tau_{sx},\tau_{yd}\}$, $\{\tau_{sy},\tau_{xd}\}$, $\{\tau_{xy},\tau_{sd}\}$. The orbital singlet basis $\{\sigma_n\}$ is given by symmetric combinations such as $\sigma_{ss'}=(ss'+s's)/\sqrt{2}$ ($s\neq s'$) and $\sigma_{ss}=ss$, and it has four subspaces $\{\sigma_{ss'},\sigma_{xx'},\sigma_{yy'},\sigma_{dd'}\}$, $\{\sigma_{sx},\sigma_{yd}\}$, $\{\sigma_{sy},\sigma_{xd}\}$, and $\{\sigma_{xy},\sigma_{sd}\}$. These subspaces are not mixed by the inversion-symmetric part of H_0. The inversion-asymmetric part of H_0 couples the singlet subspaces among themselves by terms linear in $E_{x,y}$ and the triplet subspaces among themselves. The eigenstates of H_0 have several components from different subspaces:

$$T_1=T_1^x+E_xT_1^s+E_xE_yT_1^y+E_yT_1^d,$$
$$S_3=S_3^y+E_yS_3^s+E_xE_yS_3^x+E_xS_3^d, \tag{3}$$

and similarly for T_2 and S_2. Here T_1 (T_2) labels the lowest triplet with a dominant x (y) component and S_2 (S_3) labels the lowest singlet with a dominant x (y) component. T_1^x is the projection of T_1 on the x-symmetry triplet subspace, etc. The lowest states are shown in Fig. 1(a) where $E_y=0$. Higher states not shown are T_3 (T_4), which are the lowest d- (s-) dominant triplets, and S_4 (the lowest d-dominant singlet). The isotropic part of the exchange for triplet T_i (energy ϵ_i^t) and singlet S_j (energy ϵ_j^s) is given by $J_{ij}=2(\epsilon_i^t-\epsilon_j^s)/\hbar^2$. In this work we choose the energy splitting between the electron ground and excited states to be in the range 20–45 meV; this gives an exchange splitting (J_{13} between T_1 and S_3) of the order 5–10 meV, in the range of experiments.[4]

Next, the triplet-singlet mixing comes from the SO terms $\boldsymbol{h}^V$, $\boldsymbol{h}^C$, $\boldsymbol{h}^B$ added to H_0. These give a Hamiltonian composed of a spin-symmetric part H_s that conserves the total spin $\hat{\boldsymbol{S}}=\hat{\boldsymbol{s}}_1+\hat{\boldsymbol{s}}_2$ and a spin-antisymmetric part H_a:

$$H_s=H_0+\frac{1}{2}(\hat{\boldsymbol{h}}_1+\hat{\boldsymbol{h}}_2+\gamma_s\partial_{\boldsymbol{\rho}_r}U_C\times\hat{\boldsymbol{p}}_r^{\perp})\cdot\hat{\boldsymbol{S}},$$
$$H_a=\frac{1}{2}(\hat{\boldsymbol{h}}_1-\hat{\boldsymbol{h}}_2+2\gamma_s\partial_{\boldsymbol{\rho}_r}U_C\times\hat{\boldsymbol{p}}_c^{\perp})\cdot(\hat{\boldsymbol{s}}_1-\hat{\boldsymbol{s}}_2), \tag{4}$$

where $\hat{\boldsymbol{h}}_k=\hat{\boldsymbol{h}}_k^V+\hat{\boldsymbol{h}}_k^B$, $\hat{\boldsymbol{p}}_r=\hat{\boldsymbol{p}}_1-\hat{\boldsymbol{p}}_2$, and $\hat{\boldsymbol{p}}_c=(\hat{\boldsymbol{p}}_1+\hat{\boldsymbol{p}}_2)/2$. H_a can be written as

$$H_a=\sum_{i,j}\boldsymbol{\beta}_{ij}\cdot(\hat{\boldsymbol{s}}_1-\hat{\boldsymbol{s}}_2)|T_i\rangle\langle S_j|+\text{H.c.}, \tag{5}$$

where $\boldsymbol{\beta}_{ij}=\langle T_i|\hat{\boldsymbol{h}}_1+\gamma_s\partial_{\boldsymbol{\rho}_r}U_C\times\hat{\boldsymbol{p}}_c^{\perp}|S_j\rangle$ gives the asymmetric exchange. States of different total spin $\hat{\boldsymbol{S}}$ are coupled via the operator $\hat{\boldsymbol{s}}_1-\hat{\boldsymbol{s}}_2$ equivalent to the Dzyaloshinskii-Morya form $2i/\hbar(\hat{\boldsymbol{s}}_1\times\hat{\boldsymbol{s}}_2)$.[14] We can write

$$\boldsymbol{\beta}\cdot(\hat{\boldsymbol{s}}_1-\hat{\boldsymbol{s}}_2)=\beta^z(\hat{s}_1^z-\hat{s}_2^z)+\boldsymbol{\beta}^{\perp}\cdot(\hat{\boldsymbol{s}}_1^{\perp}-\hat{\boldsymbol{s}}_2^{\perp}). \tag{6}$$

β^z conserves the total spin projection S^z, i.e., it mixes singlets with triplets with $S^z=0$ ("longitudinal mixing"). This is equivalent to a precession of the total spin around $\boldsymbol{e}_z$ ($\Delta S^z=0$). $\boldsymbol{\beta}^{\perp}$ mixes states with different spin projections ($|\Delta S^z|\neq 0$) ("transverse mixing"). The degree of triplet-singlet mixing is given by the ratio of the asymmetric to the symmetric exchange: $\mu_{ij}^z=\hbar^{-1}\beta_{ij}^z/J_{ij}$, $\boldsymbol{\mu}_{ij}^{\perp}=\hbar^{-1}\boldsymbol{\beta}_{ij}^{\perp}/J_{ij}$.

We group the operators giving $\boldsymbol{\beta}_{ij}$ in Eq. (5) into an axial vector operator $\hat{\boldsymbol{A}}\equiv\hat{A}\boldsymbol{e}_z$ and two polar vector operators $\hat{\boldsymbol{P}}\equiv\hat{P}\boldsymbol{e}_z$, $\hat{\boldsymbol{R}}\equiv\hat{\boldsymbol{R}}^{\perp}$:

$$\hat{\boldsymbol{A}}=2\gamma_s^V(\hat{\partial}_{\boldsymbol{\rho}_1}\mathcal{V}_s\times\hat{\partial}_{\boldsymbol{\rho}_1})-2\gamma_s(\partial_{\boldsymbol{\rho}_r}U_C\times\hat{\partial}_{\boldsymbol{\rho}_c}),$$
$$\hat{\boldsymbol{P}}=2\gamma_s^V(\hat{\partial}_{\boldsymbol{\rho}_1}\mathcal{V}_a\times\hat{\partial}_{\boldsymbol{\rho}_1}),$$
$$\hat{\boldsymbol{R}}=-2\gamma^V(\boldsymbol{e}_z\times\hat{\partial}_{\boldsymbol{\rho}_1})+2\gamma^B(\boldsymbol{e}_x\hat{\partial}_{x_1}-\boldsymbol{e}_y\hat{\partial}_{y_1}). \tag{7}$$

$\hat{\boldsymbol{A}}$ and $\hat{\boldsymbol{P}}$ include the vertical magnetic field from the 2D motion in the nearly degenerate excited states, and they generate β^z. $\hat{\boldsymbol{R}}$ arises from the Rashba and Dresselhaus terms, and it generates $\boldsymbol{\beta}^{\perp}$.

Table I gives the matrix elements between T_i ($i=1,4$) and S_j ($j=1,4$) [Eq. (3)] from the spin mixing operator $\hat{\boldsymbol{A}}$ in Eq. (7). The states are characterized by the symmetry of their dominant wave function components, e.g., $S_2\approx x$ symmetry. Table II gives corresponding results from $\hat{\boldsymbol{P}}$. The terms in small boxes on the second diagonal in Table I are dominant and are independent of lateral asymmetries. All the other terms in Tables I and II are nonzero only for cases of lateral asymmetry. The central 2×2 block highlighted is of interest for the dynamics of X^- in the "p" shell.[3,4]

The matrix elements in Tables I and II can be understood by writing the operators in the basis $\{\tau_m,\sigma_n\}$: $\hat{\boldsymbol{A}}+\hat{\boldsymbol{P}}=\Sigma_{m,n}(A_{mn}+P_{mn})\boldsymbol{e}_z|\tau_m\rangle\langle\sigma_n|+\text{H.c.}$ The matrix elements $A_{ij}^{\alpha\beta}$ and $P_{ij}^{\alpha\beta}$ in the tables are given by sums of matrix elements A_{mn} and P_{mn}, respectively, with the same symmetry. From Eq. (7), it is seen that A_{mn} is nonzero only for $|\tau_m\rangle\langle\sigma_n|$ odd both in x and in y. Thus $\hat{\boldsymbol{A}}$ can produce longitudinal mixing β_{ij}^z between two-electron eigenstates T_i and S_j if one of these contains an x- (s-) symmetry component, and the other has a

TABLE I. The part of the longitudinal coupling β_{ij}^{z} from $\hat{\boldsymbol{A}}$ [Eq. (7)]. The matrix elements $A_{ij}^{\alpha\beta}=\langle T_i^{\alpha}|\hat{A}|S_j^{\beta}\rangle$ are between components of definite symmetries T_i^{α}, S_j^{β} of the orbital wave functions T_i, S_j [Eq. (3)].

	S_1 ($\approx s$-symmetry)	S_2 ($\approx x$-symmetry)	S_3 ($\approx y$-symmetry)	S_4 ($\approx d$-symmetry)
T_4 ($\approx s$)	$E_xE_y[A_{41}^{xy}+A_{41}^{yx}+A_{41}^{sd}+A_{41}^{ds}]$	$E_y[A_{42}^{sd}+A_{42}^{yx}+E_x^2(A_{42}^{xy}+A_{42}^{ds})]$	$E_x[A_{43}^{sd}+A_{43}^{xy}+E_y^2(A_{43}^{xy}+A_{43}^{sd})]$	$\boxed{A_{44}^{sd}}+$ $E_x^2A_{44}^{xy}+E_y^2(A_{44}^{yx}+E_x^2A_{44}^{ds})$
T_1 ($\approx x$)	$E_y[A_{11}^{xy}+A_{11}^{ds}+E_x^2(A_{11}^{sd}+A_{11}^{yx})]$	$E_xE_y[A_{12}^{xy}+A_{12}^{yx}+A_{12}^{sd}+A_{12}^{ds}]$	$\boxed{A_{13}^{xy}}+$ $E_x^2A_{13}^{sd}+E_y^2(A_{13}^{ds}+E_x^2A_{13}^{yx})$	$E_x[A_{14}^{xy}+A_{14}^{sd}+E_y^2(A_{14}^{ds}+A_{14}^{yx})]$
T_2 ($\approx y$)	$E_x[A_{21}^{yx}+A_{21}^{ds}+E_y^2(A_{21}^{sd}+A_{21}^{xy})]$	$\boxed{A_{22}^{yx}}+$ $E_x^2A_{22}^{ds}+E_y^2(A_{22}^{sd}+E_x^2A_{22}^{xy})$	$E_xE_y[A_{23}^{xy}+A_{23}^{yx}+A_{23}^{sd}+A_{23}^{ds}]$	$E_y[A_{24}^{yx}+A_{24}^{sd}+E_x^2(A_{24}^{ds}+A_{24}^{xy})]$
T_3 ($\approx d$)	$\boxed{A_{31}^{ds}}+$ $E_x^2A_{31}^{yx}+E_y^2(A_{31}^{xy}+E_x^2A_{31}^{sd})$	$E_x[A_{32}^{ds}+A_{32}^{yx}+E_y^2(A_{32}^{xy}+A_{32}^{sd})]$	$E_y[A_{33}^{ds}+A_{33}^{xy}+E_x^2(A_{33}^{yx}+A_{33}^{sd})]$	$E_xE_y[A_{34}^{xy}+A_{34}^{yx}+A_{34}^{sd}+A_{34}^{ds}]$

y- (d-) symmetry part (Table I). P_{mn} is nonzero only for nonzero QD asymmetries ($\mathcal{V}_a\neq 0$) and for $|\tau_m\rangle\langle\sigma_n|$ odd either only in x or only in y. Thus, $\hat{\boldsymbol{P}}$ contributes to the longitudinal spin mixing β_{ij}^{z} between T_i and S_j if one of them has an s or d component and the other has an x or y component (Table II). $\hat{\boldsymbol{R}}$ can be written as $\hat{\boldsymbol{R}}=\Sigma_{m,n}\boldsymbol{R}_{mn}^{\perp}|\tau_m\rangle\langle\sigma_n|+\mathrm{H.c.}$ Results for the matrix elements of $\boldsymbol{R}_{mn}^{\perp}$ are not given explicitly here. They require QD lateral asymmetry and are nonzero for $|\tau_m\rangle\langle\sigma_n|$ odd in one of x or y. They can give transverse spin mixing $\boldsymbol{\beta}_{ij}^{\perp}$ of states with different z spin projections.

We now consider QDs with several symmetries and the longitudinal spin mixing μ^z from them. This longitudinal mixing does not have contributions from the Dresselhaus and Rashba couplings.

(i) QDs with lateral inversion symmetry ($E_x=E_y=0$). Examples are shown in Fig. 1(b) and by the $E_x=0$ points in Figs. 1(a) and 1(c) and Fig. 2(a). In such QDs, the two-electron states T_i,S_j [Eq. (3)] have well-defined symmetries. The spin mixing is due only to $\hat{\boldsymbol{A}}$ on the second diagonal (in small boxes) in Table I. "Pure" states of x (y) symmetry such as T_1 (T_2) couple only to "pure" states of y (x) symmetry such as S_3 (S_2). The first-order longitudinal spin mixing of T_1 (T_2) is given by the coupling S_3 (S_2), because this is the closest in energy. T_3 (the lowest d-symmetry triplet) couples by $\hat{\boldsymbol{A}}$ to s-symmetry singlets like S_1. T_4 (the lowest s-symmetry triplet) couples by $\hat{\boldsymbol{A}}$ to d-symmetry singlets such as S_4.

From Figs. 1(b) and 2(a) (at $E_x=0$), the asymmetric exchange can be a substantial fraction of the symmetric exchange (up to $\approx$50%). From Fig. 1(b), the asymmetric exchange is smaller for larger QDs, which results from larger orbits giving smaller effective magnetic fields in the SO coupling. In this case $\beta_{22}^{z}=-\beta_{13}^{z}$ because of degeneracy. The orbital momentum $\hat{L}_z$ eigenstates $(S_2\pm iS_3)/\sqrt{2}$ are strongly coupled to $(T_1\pm iT_2)/\sqrt{2}$ and L_z is conserved. From Fig. 2(a), the asymmetric exchange decreases as the degeneracy of the first two excited states is removed when $D_x\neq D_y$. In this case L_z is not conserved. The stronger confinement along $\boldsymbol{e}_y$ ($D_x>D_y$) leads to $J_{13}>J_{22}$, and thus to $|\mu_{13}^{z}|<|\mu_{22}^{z}|$.

(ii) QDs with a single vertical plane of reflection ($E_x\neq 0$ and $E_y=0$). This gives more nonzero matrix elements in Tables I and II, e.g., now T_4 is mixed with S_3 as well as with

TABLE II. The part of the longitudinal coupling β_{ij}^{z} from $\hat{\boldsymbol{P}}$ [Eq. (7)]. $P_{ij}^{\alpha\beta}=\langle T_i^{\alpha}|\hat{P}|S_j^{\beta}\rangle$ are between wave function components of definite symmetry [Eq. (3)].

	S_1	S_2	S_3	S_4
T_4	$E_x[P_{41}^{sx}+P_{41}^{xs}+E_y^2(P_{41}^{yd}+P_{41}^{dy})]+$ $E_y[P_{41}^{sy}+P_{41}^{ys}+E_x^2(P_{41}^{xd}+P_{41}^{ds})]$	$P_{42}^{sx}+E_x^2P_{42}^{xs}+E_y^2(P_{42}^{yd}+E_x^2P_{42}^{dy})+$ $E_xE_y(P_{42}^{sy}+P_{42}^{xd}+P_{42}^{ys}+P_{42}^{dx})$	$P_{43}^{sy}+E_x^2P_{43}^{xd}+E_y^2(P_{43}^{zys}+E_x^2P_{43}^{dx})+$ $E_xE_y(P_{43}^{sx}+P_{43}^{xs}+P_{z43}^{yd}+P_{43}^{dy})$	$E_x[P_{44}^{sy}+P_{44}^{xd}+E_y^2(P_{44}^{ys}+P_{44}^{dx})]+$ $E_y[P_{44}^{sx}+P_{44}^{yd}+E_y^2(P_{44}^{xs}+P_{44}^{dy})]$
T_1	$P_{11}^{xs}+E_x^2P_{11}^{sx}+E_y^2(P_{11}^{dy}+E_x^2P_{11}^{yd})+$ $E_xE_y(P_{11}^{xd}+P_{11}^{sy}+P_{11}^{dx}+P_{11}^{ys})$	$E_x[P_{12}^{xs}+P_{12}^{sx}+E_y^2(P_{12}^{sy}+P_{12}^{ys})]+$ $E_y[P_{12}^{xd}+P_{12}^{dx}+E_x^2(P_{12}^{sx}+P_{12}^{ys})]$	$E_x[P_{13}^{xd}+P_{13}^{sy}+E_y^2(P_{13}^{sy}+P_{13}^{dx})]+$ $E_y[P_{13}^{xs}+P_{13}^{dy}+E_x^2(P_{13}^{sx}+P_{13}^{ys})]$	$P_{14}^{xd}+E_x^2P_{14}^{sy}+E_y^2(P_{14}^{dx}+E_x^2P_{14}^{ys})+$ $E_xE_y(P_{14}^{xs}+P_{14}^{sx}+P_{14}^{dy}+P_{14}^{yd})$
T_2	$P_{21}^{ys}+E_x^2P_{21}^{dx}+E_y^2(P_{21}^{sy}+E_x^2P_{xd}^{ys})+$ $E_xE_y(P_{21}^{yd}+P_{21}^{dy}+P_{21}^{sx}+P_{21}^{xs})$	$E_x[P_{22}^{ys}+P_{22}^{dx}+E_y^2(P_{22}^{sy}+P_{22}^{xd})]+$ $E_y[P_{22}^{yd}+P_{22}^{sx}+E_x^2(P_{22}^{dy}+P_{22}^{xs})]$	$E_x[P_{23}^{yd}+P_{23}^{dy}+E_y^2(P_{23}^{sx}+P_{23}^{xs})]+$ $E_y[P_{23}^{ys}+P_{23}^{sy}+E_x^2(P_{23}^{dx}+P_{23}^{xd})]$	$P_{24}^{yd}+E_x^2P_{24}^{dy}+E_y^2(P_{24}^{sx}+E_x^2P_{24}^{xs})+$ $E_xE_y(P_{24}^{ys}+P_{24}^{dx}+P_{24}^{sy}+P_{24}^{xd})$
T_3	$E_x[P_{31}^{dx}+P_{31}^{ys}+E_y^2(P_{31}^{xd}+P_{31}^{sy})]+$ $E_y[P_{31}^{dy}+P_{31}^{xs}+E_x^2(P_{31}^{yd}+P_{31}^{sx})]$	$P_{32}^{dx}+E_x^2P_{32}^{ys}+E_y^2(P_{32}^{xd}+E_x^2P_{32}^{sy})+$ $E_xE_y(P_{32}^{dy}+P_{32}^{yd}+P_{32}^{xs}+P_{32}^{sx})$	$P_{33}^{dy}+E_x^2P_{33}^{yd}+E_y^2(P_{33}^{xs}+E_x^2P_{33}^{sx})+$ $E_xE_y(P_{33}^{dx}+P_{33}^{ys}+P_{33}^{xd}+P_{33}^{sy})$	$E_x[P_{34}^{dy}+P_{34}^{yd}+E_y^2(P_{34}^{xs}+P_{34}^{sx})]+$ $E_y[P_{34}^{dx}+P_{34}^{xd}+E_x^2(P_{34}^{ys}+P_{34}^{sy})]$

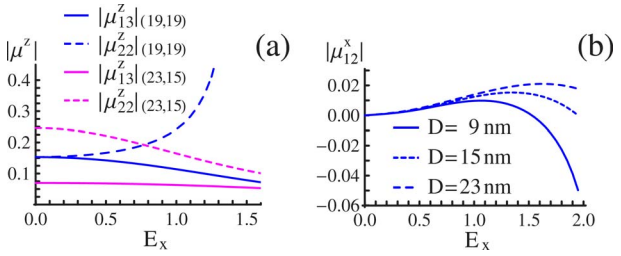

FIG. 2. (Color online) (a) μ^z in QDs with D_x=23 nm and D_y =15 nm compared to the longitudinal coupling in QDs with D_x $=D_y$=19 nm. (b) Mixing of states with different spin projections S^z in QDs with $D_x=D_y$ and with a plane of symmetry (E_y=0, $E_x\neq 0$): μ^x_{12} for the mixing of T_1 and S_2.

S_4. This case corresponds to Figs. 1(a), 1(c), and 2(a). μ^z_{13} for the lowest triplet decreases with increasing E_x. For these cases, the terms proportional to E_x and E_x^2 in Table I and also the terms from $P=2\tilde{\gamma}^V(\partial_{\boldsymbol{\rho}_1}\mathcal{V}_{ax}\times\hat{\partial}_{\boldsymbol{\rho}_1})^z_{mn}\propto E_x$ from Table II are nonzero, and they tend to cancel partially the larger terms in the boxes in Table I. For some triplet-singlet pairs, such as S_3 and T_1, the symmetric exchange becomes larger and thus their mixing decreases. Other singlet-triplet pairs can be degenerate, such as T_2 and S_2 in Fig. 1(a) at $E_x\approx 1.5$; then a nonzero β^z_{22} leads to strong singlet-triplet mixing (Fig. 2(a)). For this case, L_z is not conserved. Triplets with $\langle\hat{L}_z\rangle\approx\pm\hbar$ can be coupled to singlets that have $\langle\hat{L}_z\rangle\approx\mp\hbar$.

(iii) QDs with no vertical plane of reflection ($E_x\neq 0$ and $E_y\neq 0$). Then all states in Tables I and II are mixed, and the longitudinal spin mixing can be larger than in previous cases.

In addition to the longitudinal spin mixing above, there is also mixing that changes the spin projection S^z (transverse mixing $\boldsymbol{\mu}^\perp$). It is exclusively from the Dresselhaus and Rashba couplings, which give $\boldsymbol{R}$ in Eq. (7). For lateral inversion symmetry, $\boldsymbol{R}$ mixes states which typically differ by the single-particle energy splitting, e.g., T_1 with S_1 and S_4, etc. Then the mixing from $\hat{\boldsymbol{R}}$ is small, due to large J_{11} and J_{14}. For QDs with only one vertical plane of reflection, $\hat{\boldsymbol{R}}$ mixes T_1 with S_2 or S_3, which are closer in energy and therefore give larger mixing. We show in Fig. 2(b) this transverse spin mixing for T_1 and S_2. It occurs only for nonzero asymmetric potential ($E_x\neq 0$). It is generally smaller than the longitudinal spin mixing but can become appreciable for large asymmetries, and it is larger in smaller QDs.

We have shown that when the splitting between the electron p-states in a QD is small there can be strong mixing between electron excited singlets and triplets. This mixing can be important in optical manipulations of spins in QDs and can lead to dephasing and loss of fidelity in gates. For example, these results can help in interpretations of light polarization reversal experiments. These interpretations involve electron singlet-triplet mixing. A contribution to the latter comes from *e-h* axially-asymmetric exchange in laterally asymmetric QDs. The *e-e* asymmetric exchange presented here provides an additional contribution, which is important in particular for laterally symmetric QDs. The present results also suggest an additional process in such experiments. Typically in optical pumping, the orbital angular momentum from light is stored in the hole motion and the electron is in an s state. For states with an excited electron, the electrons can carry the orbital angular momentum. The *e-e* asymmetric exchange can mix two-electron states that differ in their orbital angular momentum leading to emission of light with reversed polarization.

Finally, in gated QDs, which are typically larger, the mixing discussed here between triplets and excited singlets is smaller [Fig. 1(b)]. Nevertheless, in situations like spin transport with a bias through gated QDs,[15] the lowest singlet can be brought close to the ground state singlet and the mixing between them can become important.

We are grateful for discussions with Y. Lyanda-Geller, D. Gammon, B. V. Shanabrook, and M. E. Ware. This work was supported in part by the ONR and by DARPA.

[1] D. Loss and D. P. DiVincenzo, Phys. Rev. A **57**, 120 (1998).
[2] M. Kroutvar *et al.*, Nature (London) **432**, 81 (2004).
[3] S. Cortez *et al.*, Phys. Rev. Lett. **89**, 207401 (2002).
[4] M. E. Ware *et al.*, Phys. Rev. Lett. **95**, 177403 (2005).
[5] V. B. Berestetskii, E. M. Lifsitz, and L. P. Pitaevskii, *Quantum Electrodynamics* (Butterworth-Heinemann, London, 1998).
[6] G. L. Bir and G. E. Pikus, *Symmetry and Strain-Induced Effects in Semiconductors* (John Wiley & Sons, New York, 1974).
[7] The Kane model (Ref. 6) uses the following parameters: band gap E_g, energy of the split-off band Δ, and matrix element P of operator $\hbar\hat{p}_x/m_0$ between the conduction and valence bands.
[8] $\gamma^V_s=-\frac{c_h}{\hbar^2}\frac{2P^2}{3E_g^2}\frac{\Delta(2E_g+\Delta)}{(E_g+\Delta)^2}$ comes from the mixing of the $\boldsymbol{k}\cdot\hat{\boldsymbol{p}}$ terms with the hole potential $V_h=c_hV$ ($0<c_h<1$). The procedure is similar to that for the Coulomb interaction (Ref. 11).
[9] Yu. L. Bychkov and E. I. Rashba, JETP Lett. **39**, 78 (1984).
[10] γ^V contains the discontinuities at the material interfaces and the effective electric field in the QD along $\boldsymbol{e}_z$. See, e.g., P. Pfeffer and W. Zawadzki, Phys. Rev. B **59**, R5312 (1999).
[11] Ş. C. Bădescu, Y. B. Lyanda-Geller, and T. L. Reinecke, Phys. Rev. B **72**, 161304(R) (2005): $\gamma_s=\frac{1}{\hbar^2}\frac{2P^2}{3E_g^2}\frac{\Delta(2E_g+\Delta)}{(E_g+\Delta)^2}$ comes from the combination of the $\boldsymbol{k}\cdot\hat{\boldsymbol{p}}$ terms and the Coulomb potential, also giving a correction to U_C: $\gamma_c\delta(\boldsymbol{r})$, with $\gamma_c=2\pi\frac{e^2}{\varepsilon}\frac{2P^2}{3E_g^2}\frac{(E_g+\Delta)^2+E_g^2}{(E_g+\Delta)^2}$.
[12] G. Dresselhaus, Phys. Rev. **100**, 580 (1955). This SO coupling gives $\hat{\boldsymbol{h}}^{\mathrm{B}}\cdot\hat{\boldsymbol{s}}=\gamma_b^B\epsilon^{\alpha\beta\delta}\hat{p}_\alpha(\hat{p}_\beta^2-\hat{p}_\delta^2)\hat{s}_\alpha$ in bulk.
[13] We consider dots of height W with confining potential $V(\boldsymbol{r})=-U_0\theta(|z-W/2|)(1+E_zz)\tilde{\mathcal{V}}(\boldsymbol{\rho})$ where U_0 is the conduction band offset and θ is the step function. Here we take W=4 nm and InAs/GaAs band parameters with U_0=0.6 eV. The vertical function $\xi(z)$ is the solution of $V_z(z)=-U_0\theta(|z-W/2|)(1+E_zz)$. We take the principal axes $\boldsymbol{e}_{x,y}$ of the QD to be along the crystal axes [110] and [1$\bar{1}$0]. The lateral potential $\mathcal{V}(\boldsymbol{\rho})=-U_0\tilde{\mathcal{V}}(\boldsymbol{\rho})$ has an inversion-symmetric part $\mathcal{V}_s(\boldsymbol{\rho})=-U_0e^{-(2x/D_x)^2-(2y/D_y)^2}$ and an inversion-antisymmetric part $\mathcal{V}_a(\boldsymbol{\rho})=\mathcal{V}_s(\boldsymbol{\rho})\left[E_x\left(\frac{2x}{D_x}\right)^3+E_y\left(\frac{2y}{D_y}\right)^3\right]$ $=\mathcal{V}_{ax}(\boldsymbol{\rho})+\mathcal{V}_{ay}(\boldsymbol{\rho})$.The average electric field is $\mathcal{E}_{x,y}=-\partial_{x,y}\mathcal{V}_a$ $\approx 0.32U_0E_{x,y}/D_{x,y}$.
[14] I. E. Dzyaloshinskii, Phys. Chem. Solids **4**, 241 (1958); T. Morya, Phys. Rev. **120**, 91 (1960).
[15] R. Hanson *et al.*, Phys. Rev. B **70**, 241304(R) (2004); F. Mireles *et al.*, Appl. Phys. Lett. **88**, 093118 (2006).